

Direct Measurement of the Delay Time Distribution of Type Ia Supernovae by the Subaru/XMM-Newton Deep Survey and Implications for the Progenitor

Tomonori TOTANI¹, Tomoki MOROKUMA², Takeshi ODA¹, Mamoru DOI³, and Naoki YASUDA⁴

¹*Department of Astronomy, School of Science, Kyoto University, Sakyo-ku, Kyoto 606-8502*

²*National Astronomical Observatory, 2-21-1 Osawa, Mitaka, Tokyo, 181-8588*

³*Institute of Astronomy, School of Science, The University of Tokyo, 2-21-1 Osawa, Mitaka, Tokyo, 181-0015*

⁴*Institute for Cosmic Ray Research, The University of Tokyo, Kashiwa, Chiba, 227-8582*

(Received ; accepted)

Abstract

The delay time distribution (DTD) of type Ia supernovae (SNe Ia) from star formation is an important clue to reveal the still unknown progenitor system of SNe Ia. Here we report a direct measurement of the SN Ia DTD by using the faint variable objects detected in the Subaru/XMM-Newton Deep Survey (SXDS) down to $i' \sim 25.5$. We select 65 SN candidates showing significant spatial offset from nuclei of the host galaxies having old stellar population at $z \sim 0.4\text{--}1.2$, out of more than 1,000 SXDS variable objects. Although spectroscopic type classification is not available for these, we quantitatively demonstrate that more than $\sim 80\%$ of these should be SNe Ia. The DTD is derived using the stellar age estimates of the old galaxies based on 9 band photometries from optical to mid-infrared wavelength, and it is well described by a featureless power-law as $f_D(t_{\text{Ia}}) \propto t_{\text{Ia}}^\alpha$ with $\alpha \sim -1$ in a delay time range of $t_{\text{Ia}} = 0.1\text{--}10$ Gyr. This DTD shape is in excellent agreement with the generic prediction of the double-degenerate scenario, giving a strong support to this scenario. In the single-degenerate (SD) scenario, although predictions by simple analytic formulations have broad DTD shapes that are similar to the observation, DTD shapes calculated by more detailed binary population synthesis tend to have strong peaks at characteristic time scales that do not fit the observation. This result thus indicates either that the SD channel is not the major contributor to SNe Ia in old stellar population, or that improvement of binary population synthesis theory is required. Various sources of systematic uncertainties are examined and tested, but our main conclusions are not changed significantly.

Key words: stars: supernovae: general — galaxies: evolution — cosmology: observations

1. Introduction

It is widely believed that type Ia supernovae (SNe Ia) are thermonuclear explosions of white dwarfs in binary systems, triggered when the mass of a white dwarf grows up to the Chandrasekhar mass by accretion from its companion (see Nomoto et al. 1997; Hillebrandt & Niemeyer 2000; Livio 2001 for reviews). However, the progenitor binary system leading to SNe Ia is still unknown, and there are two competing scenarios for the accretion process that triggers SNe Ia. In the single-degenerate (SD) scenario, the accretion is from a non-degenerate companion star (Whelan & Iben 1973; Nomoto 1982), while in the double-degenerate (DD) scenario, a merger of two white dwarfs whose total mass is exceeding the Chandrasekhar mass results in a SN Ia (Iben & Tutukov 1984; Webbink 1984). To reveal the progenitor is important not only for better understanding of this one of the brightest explosions in the universe, but also for controlling systematic uncertainties when SNe Ia are used as a standard candle to measure the expansion rate of the universe (Riess et al. 1998; Perlmutter et al. 1999). SNe Ia are expected to have a wide range of delay time from star formation

to supernova explosions, and the delay time distribution (DTD) can be used to discriminate the proposed progenitor models, since different progenitor scenarios predict different DTDs.

The DTD is equivalent to the SN Ia occurrence rate evolution as a function of the stellar age in a single starburst stellar population system, and observational studies on SN Ia rates should be able to constrain DTD (Mannucci et al. 2006 and references therein). One such approach is to examine the evolution of the cosmic SN Ia rate density (Gal-Yam & Maoz 2004; Maoz & Gal-Yam 2004; Strolger et al. 2004; Dahlen et al. 2004; Barris & Tonry 2006; Förster et al. 2006; Oda et al. 2008; Blanc & Greggio 2008). However, there is a degeneracy between SN Ia DTD and the cosmic star formation history, and it is difficult to derive a strong constraint on DTD from the currently available data (Förster et al. 2006; Oda et al. 2008; Blanc & Greggio 2008). Another approach is to study the dependence of SN rate on the host galaxy properties (Mannucci et al. 2005; Scannapieco & Bildsten 2005; Sullivan et al. 2006; Aubourg et al. 2007). The dependence of SN Ia rate on the color or spectral energy distribution (SED) of host galaxies gives useful constraints on DTD, indicating the

existence of SN Ia populations having short ($\lesssim 0.1$ Gyr) and long ($\gtrsim 10$ Gyr) delay times. However, the functional shape of the DTD, $f_D(t_{\text{Ia}})$, as a function of the delay time t_{Ia} has not yet quantitatively been constrained well.

For a direct DTD measurement, one needs to reliably estimate the delay time of an observed SN Ia and the stellar mass of its host galaxy. The mean stellar age of the host galaxy is an indicator of the delay time, but it is unreliable when the stellar age distribution has a large dispersion compared with the mean age. The ideal population for this purpose is old galaxies with an approximately uniform stellar age, which experienced major star formation episode in the past and have little or no star formation activity at the time of a SN explosion. Present-day elliptical galaxies are good examples, but they have a typical age of $\gtrsim 10$ Gyr (Barber et al. 2007; Jimenez et al. 2007), and hence we need to observe SNe at higher redshifts to get a sample of SNe having shorter delay times. However, both detection of SNe and stellar age estimate of host galaxies become difficult at high redshifts.

The Subaru/XMM-Newton Deep Survey (SXDS, Furusawa et al. 2008), which is the deepest survey among those wider than $\sim 1 \text{ deg}^2$ with a broad coverage of various wavelengths, provides a unique data set for this purpose. In optical bands, this field has been observed repeatedly with some time intervals, and a systematic variable object search has been performed (Morokuma et al. 2008a, b), leading to detection of more than 1,000 variable objects down to a limiting variability magnitude of $m_{i'} \sim 25.5$ (AB). The majority of them are high- z supernovae and active galactic nuclei (AGNs). This data set includes many passively evolving old galaxies at $z \sim 1$, which are believed to be the direct ancestors of the present-day elliptical galaxies (Yamada et al. 2005). We can reliably estimate the stellar age and stellar mass of host galaxies by photometric redshift calculations using the rich photometric data in the 9 band filters ($BVR_c i'z'JK$, 3.6, and $4.5 \mu\text{m}$).

In this paper we directly measure the SN Ia DTD by selecting the SXDS variable objects found in old or passively evolving galaxies at $z \sim 0.4\text{--}1.2$, and compare the measured DTD with the existing theoretical DTD predictions to get implications for the SN Ia progenitor. Spectroscopic type confirmation is not available for the faint SXDS variable objects. It is difficult to construct a complete high-redshift SN sample with spectroscopic type classification under homogeneous conditions of spectroscopic observation, and contamination of SNe with no or poor spectroscopic data is one of the most challenging sources of uncertainty in SN rate studies (Strolger et al. 2004; Sullivan et al. 2006; Poznanski et al. 2007). Here, instead of using spectroscopic information, we select variable objects in old galaxies with spatial offset from the galactic centers, and hence they are mostly expected to be SNe Ia. In fact, we will quantitatively demonstrate that the majority ($\gtrsim 80\%$) of them should be SNe Ia based on the properties of the SN candidates and their host galaxies.

It should be noted that selecting SNe only in a particular type of galaxies does not induce bias in the DTD es-

timates, since we measure SN Ia rate normalized per unit stellar mass of host galaxies having the same type. This is in contrast to measurements of total cosmic SN rate density, in which selection of any particular galaxy type obviously leads to an underestimate of the total rate.

In section 2, we describe the SXDS data set and selection procedures of old galaxies and SN candidates. In section 3, we describe the formulations of DTD measurement and present the results. In section 4, we examine various systematic uncertainties in our DTD estimates. We then discuss about the implications for the SN Ia progenitor, from the comparison between the measured DTD and theoretical predictions (section 5). Conclusions are given in section 6 with some discussions. Throughout the paper, we use the AB magnitude system and the standard Λ CDM cosmological parameters of $(h, \Omega_M, \Omega_\Lambda) = (0.7, 0.27, 0.73)$, where $h \equiv H_0/(100 \text{ km/s/Mpc})$.

2. The SXDS SN Ia Candidates

2.1. the SXDS Data and Photometric Redshift Calculations

We utilize the rich photometric data set of SXDS in $BVR_c i'z'$ bands obtained by the Subaru/Suprime-Cam (Furusawa et al. 2008), in JK bands obtained by the UKIDSS survey (Warren et al. 2007), and in 3.6 and $4.5 \mu\text{m}$ bands obtained by the SWIRE survey (Lonsdale et al. 2004), with the limiting magnitudes (3σ) of 28.4, 27.8, 27.7, 27.7, 26.6, 24.1, 24.0, 23.1, and 22.4, respectively, for aperture diameters of 2 (optical and JK) and 3.8 (the Spitzer bands) arcsec. The point-spread-function size of the optical images is about 0.8 arcsec FWHM (1 pixel = 0.2 arcsec). The total survey area used in the variable object survey (Morokuma et al. 2008a) is 0.918 deg^2 . Though the JK data is available only for about half of the SXDS field, almost all of the SXDS field is covered by the Spitzer data. This is important for reliable stellar mass estimate, which is crucial for a study of SN Ia DTD. Therefore we select relatively bright 45,374 galaxies with $m_{i'} \leq 24.0$ and $m_{3.6\mu\text{m}} \leq 22.8$, for reliable photo- z and stellar mass/age estimations. Stars have been removed by the $m_{R_c} - m_{i'}$ versus $m_{R_c} - m_{3.6\mu\text{m}}$ plot as in Morokuma et al. (2008a).

Photometric redshift (z_{ph}) calculations are performed by using the publicly available code *hyperz* (Bolzonella, Miralles, & Pell 2000), with the GALAXEV library (Bruzual & Charlot 2003) of stellar population synthesis models based on the Padova 1994 evolutionary tracks. In our baseline analysis, we use the library assuming the Salpeter initial mass function (IMF) in the mass range of $0.1\text{--}100 M_\odot$ and a supersolar abundance of $Z = 0.05$, since galaxies with old stellar population are expected to have high metallicity (Barber et al. 2007; Jimenez et al. 2007). We use 7 galaxy SED templates having exponentially decaying star formation history with the exponential time scales of $\tau_{\text{SF}} = 0.1, 0.3, 0.7, 1, 3, 5$, and 15 Gyrs. We also add a template with a constant star formation rate (SFR), and hence 8 SED templates are used in total. Attenuation of galaxy spectra by dust is taken into account with the

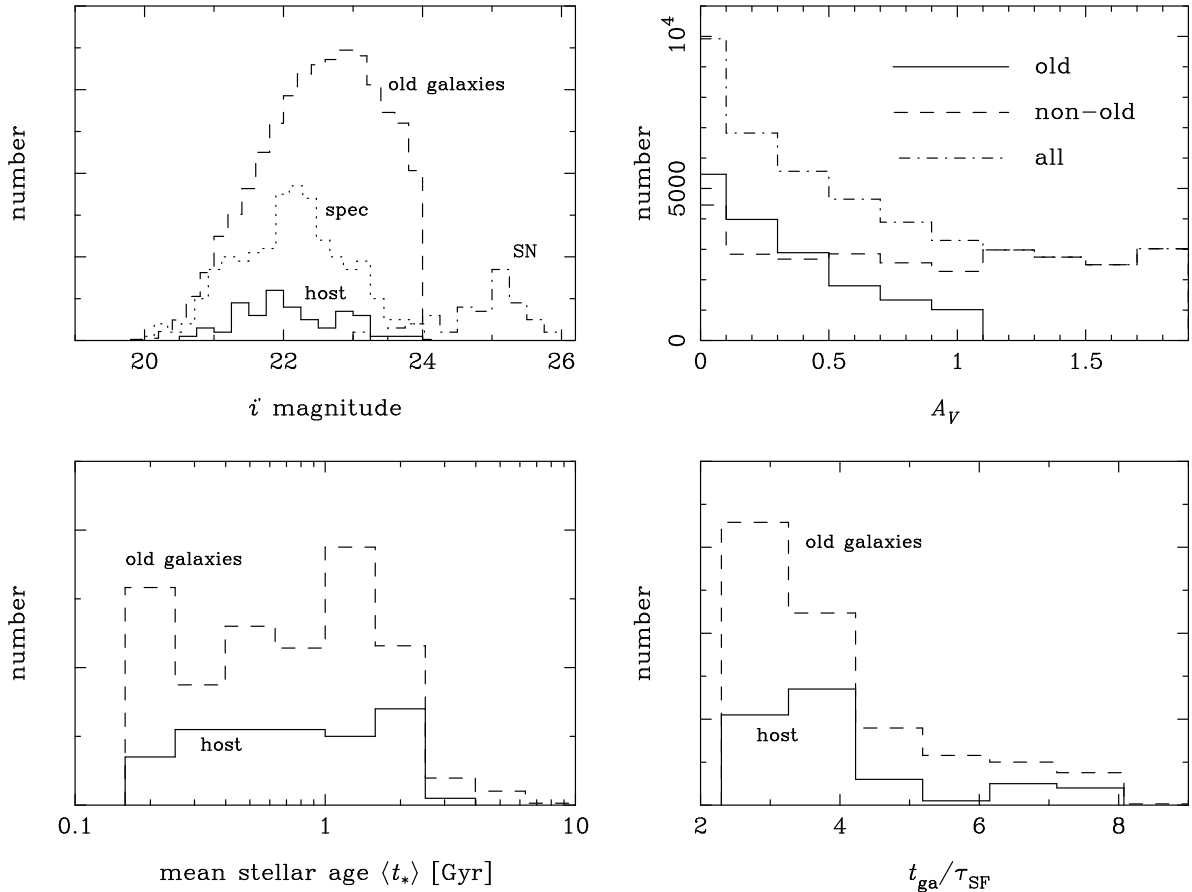


Fig. 1. The properties of the old galaxies selected for the SN search. Upper left panel: the i' -band flux distributions of the variability of the 65 SN candidates (dot-dashed line), their host galaxies (solid), the 314 old galaxies with spectroscopic data (dotted), and all the 16,492 old galaxies used in the analysis (dashed). Upper right panel: the A_V distributions of the old galaxies (solid), non-old galaxies (dashed), and all galaxies (dot-dashed) with $m_{i'} \leq 24.0$ and $m_{3.6\mu m} \leq 22.8$. Lower panels: the distributions of the mean stellar age and t_{ga}/τ_{SF} of all old galaxies (dashed) and the host galaxies of the SN candidates (solid). The normalizations of the histograms are arbitrarily scaled for presentation except for the upper-right panel.

Calzetti law (Calzetti et al. 2000) within a range of $A_V = 0-2$, where A_V is the restframe visual band attenuation. Recycling is not taken into account, and hence the stellar mass in this work means the integration of SFR over time, which is not exactly the same as the total stellar mass at a given time.

2.2. Old Galaxy Selection

For an efficient selection of SNe Ia, we must select old or passively evolving galaxies. We therefore select galaxies with $t_{ga}/\tau_{SF} > 2.3$, where t_{ga} is the galaxy age estimated by the *hyperz* code, i.e., the time elapsed from the beginning of the template star formation history. This value is chosen so that galaxies selected by this criterion have formed more than $[1 - \exp(-2.3)] = 90\%$ of stars that the galaxies would form in all the history. We also set a constraint of $A_V \leq 1.0$ to avoid dusty objects. After selecting galaxies within $0.4 \leq z_{ph} \leq 1.2$, which is a typical redshift range expected for SNe Ia detectable in SXDS, there remain 16,492 galaxies. We call these galaxies simply “the old galaxies” in this work for convenience. The distributions of i' magnitude, A_V , mean stellar age $\langle t_* \rangle$, and

t_{ga}/τ_{SF} of these old galaxies are shown in Fig. 1. As expected for old galaxies, the distribution of A_V is peaked at $A_V = 0$, with a mean value of $\langle A_V \rangle = 0.31$. The concentration to small A_V values is obvious when it is compared with the distribution of the non-old galaxies.

To test the reliability of photo- z , we compare the results with the spectroscopic redshifts (z_{sp}) of the 314 old galaxies having observed spectra in Fig. 2. The agreement is within $\pm 20\%$ for the majority of the old galaxies. The magnitude distribution of the spectroscopic sample peaks at $m_{i'} \sim 22-23$ and extends down to $m_{i'} \sim 24$ (Fig. 1), and hence our photometric old galaxy sample is restricted to the magnitude range where the spectroscopic calibration is possible. For visual demonstrations, we randomly selected 8 objects as examples from our final sample of SN candidates. The properties of the 8 objects are summarized in Table 1. The host galaxy images and the SED fits of the 8 objects are shown in Figs. 3 and 4, respectively. The photometric errors are very small especially in the optical bands since we selected bright objects, but still the agreement between the template SEDs and the observed data is quite good, which is an encouraging result about

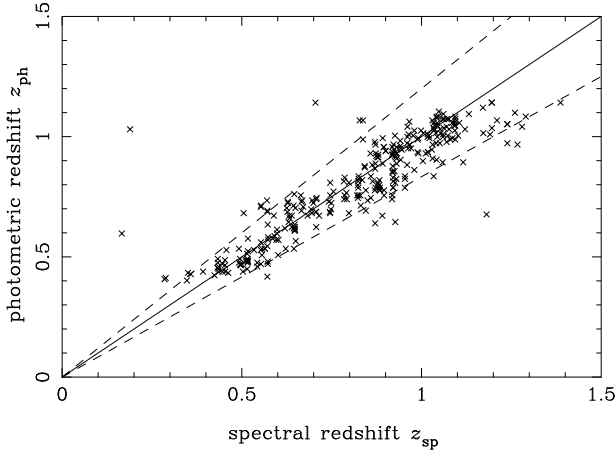


Fig. 2. Spectral redshift versus photometric redshift of the old galaxies selected for the SN Ia search. The dashed lines indicate the $\pm 20\%$ accuracy region.

the reliability of age and stellar mass estimates.

2.3. Selection of the SN Candidates

We now search for variable objects associated with these old galaxies. There are 1040 variable objects selected by i' band variability in the catalog of Morokuma et al. (2008a). The SXDS field was monitored 8–10 times during about four years, with a typical time interval from a few days to one month within a year. The variable sources are selected if it is detected in the subtracted images of any pair of two different epochs. The detection efficiency of variable sources has been carefully determined by simulations.

We select variable objects within the detection isophote (i.e., the area where the surface brightness is larger than the threshold level of the source detection) of the old galaxies, and showing significant offsets (≥ 1.9 pixel = $0.38''$) from the nuclei of galaxies. Here, the nuclei of galaxies are simply defined by their surface brightness peaks. According to the simulations using artificial objects (Morokuma et al. 2008a), this is a conservative limit to remove variable objects at nuclei of the host galaxies, i.e., AGNs. Morokuma et al. classified the nuclear variable sources into SNe or AGNs based on the light-curve shape, and they found that such classifications are broadly consistent with the X-ray information. However, the classification is rather uncertain especially for the faintest variable objects near the detection limit. Therefore we conservatively reject all nuclear variable sources. We do not use the X-ray information in the process of SN candidate selection, since a small part ($\sim 10\%$) of the survey area is not covered by the X-ray observation. Galaxies detected in the X-ray band are only 68 out of the 14,909 old galaxies observed in X-ray, which is a negligible fraction in our analysis. In fact, we confirmed that no object is detected in X-ray in our final SN candidate sample.

We thus found 67 variable objects associated with the old galaxies. We examined the optical variability information of these objects by using the full Suprime-Cam

data set of the SXDS. We found that, as expected, most of them are consistent with SN-like variability. Only 2 objects show clearly AGN-like variability, i.e., flaring up more than twice during the four year observation duration. These two are removed, leaving the 65 SN candidates. Such a contamination of AGNs is possible by a chance superposition of a normal galaxy and an unrelated AGN along the line of sight. We found that two such events are reasonable from the number of AGNs in SXDS and the area covered by the old galaxies selected here (2.3% of the total survey area). We cannot exclude a possibility that a few more AGNs whose light curves are similar to those of SNe might be included in the 65 SN candidates. To check this, we examine the offset distribution of these objects with respect to the surface brightness profile of galaxies as follows.

2.4. Radial Distribution of SN Candidates in Host Galaxies

We performed ellipsoidal fits for each galaxy with the Sérsic type radial profile (Sérsic 1968). The effective radius along the major and minor axes, and the Sérsic index are thus derived, taking into account the seeing. We then calculated the fraction, f_l , of i' -band light enclosed within the ellipsoidal radius to a variable object, compared with the total flux within the detection isophote (i.e., isophotal flux). Here, the nuclear region within the offset threshold (1.9 pixel radius) is excluded in the f_l calculation. If we are selecting SNe physically associated with the galaxies, we expect that the distribution of f_l is uniform between 0–1. The distributions of the offsets from nuclei and f_l are shown for the 65 SN candidates in Fig. 5, and in fact we find an almost uniform distribution.

There is a deficit at $f_l \gtrsim 0.8$, and it may indicate that our profile fitting is not perfect or supernova locations do not exactly trace galactic i' -band light. However, it is clear that the SN candidates trace the galactic light reasonably well, and hence the majority of these must be SNe physically associated with host galaxies, rather than the chance superpositions of background AGNs. It should be noted that, if there is a significant contamination of AGN chance superpositions, we expect a distribution biased to larger values of f_l , which is opposite from the observed trend. We thus define these 65 objects as the final SN candidate sample, and the distributions of variability and host galaxy magnitudes are shown in Fig. 1. The variability magnitude here is defined by the maximum flux difference among time intervals of all possible pairs of two different epochs observed by the Suprime-Cam. The images of the randomly selected eight examples are shown in Fig. 3.

In the final SN sample, 7 SN candidates have measured spectroscopic redshifts of host galaxies. We confirmed that the difference between z_{sp} and z_{ph} is within $\sim 20\%$ for all of these, as expected from Fig. 2. The fraction of available spectroscopic redshifts, 7/65, is considerably higher than 314/16492 for the old galaxies. This is mainly because the host galaxies of the SN candidates are systematically brighter than the typical old galaxies (see Fig. 1),

Table 1. Properties of the eight examples randomly selected from the final 65 SN sample. The redshifts are spectroscopic when available (objects 2 and 4), and otherwise photometric. Magnitudes of host galaxies and SN variability are in i' band, and galaxy age (t_{ga}), the exponential decay time scale of SFR (τ_{SF}), and mean stellar age ($\langle t_* \rangle$) are all in Gyr.

Obj. No.	redshift	host mag.	var. mag.	t_{ga}	τ_{SF}	$\langle t_* \rangle$	A_V
1	0.47	22.5	25.4	2.30	1.0	1.56	0.2
2	0.63	21.6	24.6	0.36	0.1	0.27	0.0
3	0.81	23.0	25.8	0.72	0.1	0.62	0.8
4	0.92	22.6	24.2	1.02	0.3	0.75	0.0
5	1.01	23.7	24.5	0.72	0.1	0.62	0.2
6	0.60	22.0	23.5	3.50	0.7	2.82	0.6
7	0.70	23.0	25.2	0.72	0.3	0.49	0.0
8	0.47	21.3	25.1	1.02	0.3	0.75	0.0

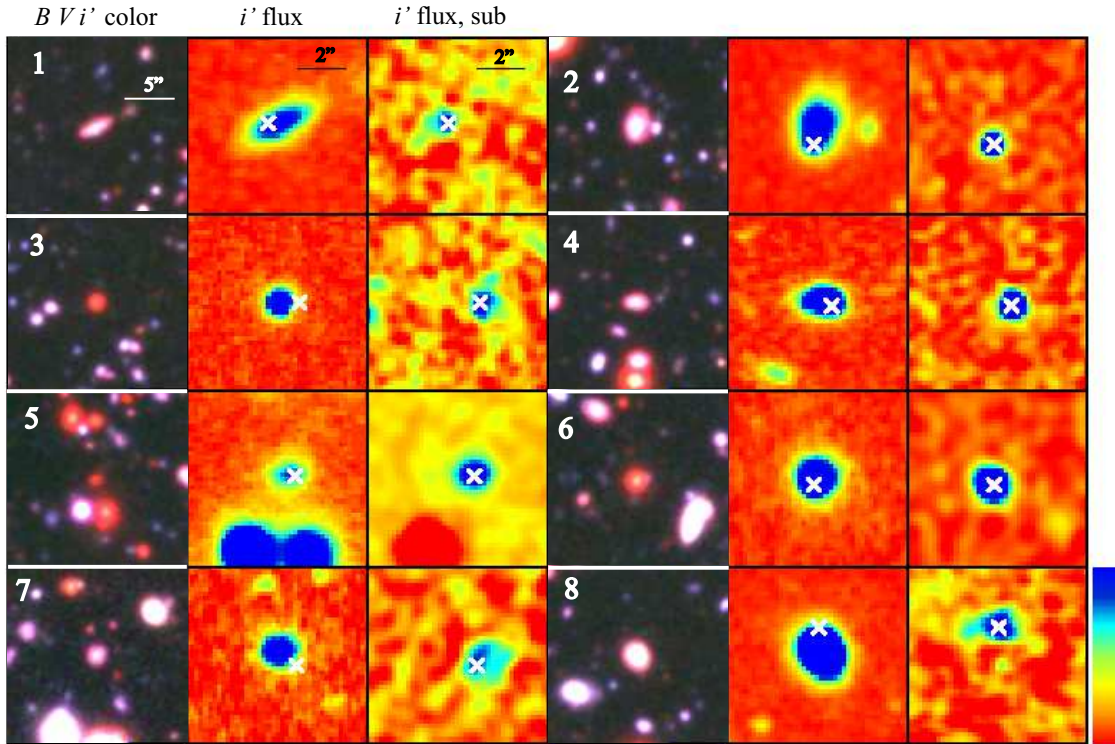


Fig. 3. The images of the eight examples randomly selected from the final SN candidates. The left panels are the 3-color composite images of the host galaxies using BVi' bands. The middle panels are color contours of the host galaxy i' band flux at the time of the maximum luminosity of the SN candidates, and the right panels are those of subtracted images showing the variability of the SN candidates. All panels are centered at the surface brightness peak of the host galaxies, and the location of the SN candidates are indicated by white crosses. The properties of the eight objects are summarized in Table 1.

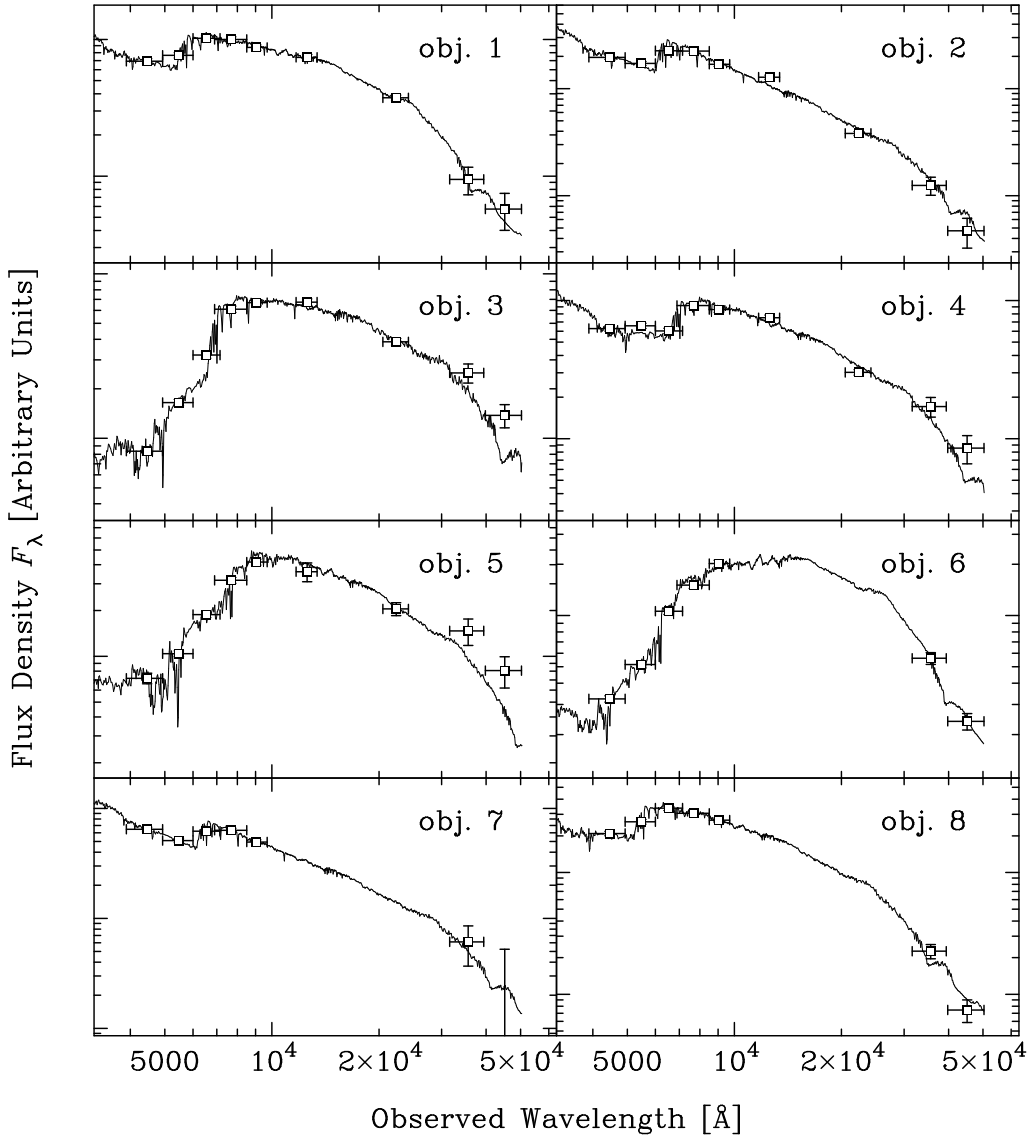


Fig. 4. The results of the SED fits of the old galaxies by the photometric redshift calculations, for the 8 example objects listed in Table 1. The open squares are the observed flux. The horizontal error bars indicate the width of band filters, and the vertical error bars are 1σ flux errors. (The flux errors are small and difficult to see in optical bands.)

reflecting the fact that SN rate is roughly proportional to host galaxy luminosities. Another possible reason is that some variable objects were followed up by spectroscopic observations as a part of the Supernova Cosmology Project in collaboration with the SXDS project. In the DTD analysis below, we use spectroscopic redshifts of the SN candidates or the old galaxies when available, and otherwise use photometric redshifts.

3. Measurement of Delay Time Distribution

3.1. The Basic Formulations

Now we estimate the DTD from the 65 SN candidates. Later (section 4) we will demonstrate that the majority of them must be SNe Ia rather than CC SNe, but here we first estimate the DTD, taking into account the contamination of CC SNe. We implicitly assume that DTD

is universal for all stellar populations, as often assumed in studies on the SN Ia DTD. It is possible that DTD is dependent on the properties of stellar population such as metallicity (Kobayashi et al. 1998), and in such a case our measurement of DTD applies only to the old galaxies selected here. This point should be kept in mind when a comparison is made with theoretical predictions.

Since we know the star formation history of the template galaxy evolution model in the *hyperz* fit, we can estimate the mass-weighted mean stellar age of galaxies, $\langle t_* \rangle$. Since we selected old galaxies, in which most of stars have formed in a starburst in the past, $\langle t_* \rangle$ is expected to be a good estimator of the delay time, t_{Ia} , of SNe Ia. The DTD function $f_D(t_{\text{Ia}})$ (per unit mass of star formation and unit delay time) can be estimated as the SN Ia rate per unit stellar mass in these galaxies. Therefore the first rough estimate of the mean DTD function \bar{f}_D in a given

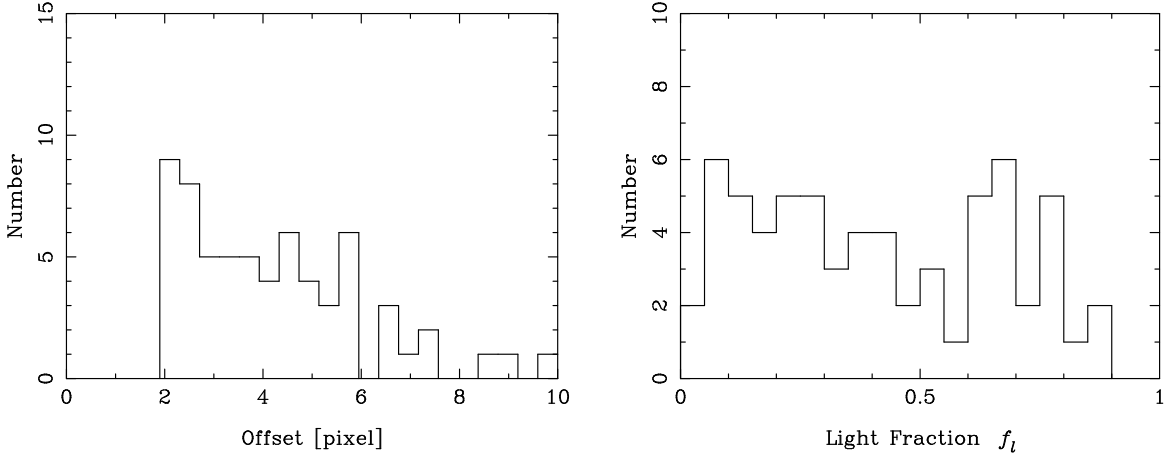


Fig. 5. Left panel: The distribution of the spatial offsets of the 65 SN candidates from the nuclei of their host galaxies. Right panel: The distribution of the fraction of galactic light f_l enclosed within the ellipsoidal radius to a SN candidate in the isophotal flux of its host galaxy.

bin of $t_l \leq t_{\text{Ia}} < t_u$ can be obtained by solving the following equation:

$$N_{\text{Ia,exp}} + N_{\text{CC,exp}} = N_{\text{obs}} , \quad (1)$$

where $N_{\text{Ia,exp}}$ and $N_{\text{CC,exp}}$ are the expected numbers of Ia and CC SNe, respectively, and N_{obs} is the number of the observed SN candidates associated with the old galaxies satisfying $t_l \leq \langle t_* \rangle < t_u$. We can calculate $N_{\text{Ia,exp}}$ as:

$$N_{\text{Ia,exp}} = \bar{f}_D \sum_i f_{\text{off},i} M_{*,i} \frac{T_{V,\text{Ia}}(z_i)}{(1+z_i)} , \quad (2)$$

where $M_{*,i}$ and z_i are the stellar mass and redshift of i -th galaxy, $f_{\text{off},i}$ the fraction of light outside the threshold offset (1.9 pixel radius), and the summation is for all the old galaxies satisfying $t_l \leq \langle t_* \rangle < t_u$.

The visibility time T_V , which is the total integrated time during which a SN can be detected by the SXDS survey, can be calculated as:

$$T_V(z) = \int_{-\infty}^{\infty} P_{\text{det}}(t, z) dt , \quad (3)$$

where t is the explosion time of a supernova relative to the SXDS observation campaign (in observer's frame), and $P_{\text{det}}(t, z)$ is the detection probability of the supernova at redshift z . The factor $(1+z_i)^{-1}$ in eq. (2) corrects the cosmological time dilation effect. This is the standard quantity in SN rate analyses, and it can be calculated if the SN light curve is given in the observing band filter. The exact procedure and efficiency of variable object detection in SXDS (Morokuma et al. 2008a) are also taken into account to calculate P_{det} . We apply the standard light curve and color evolution of SNe Ia used in Oda & Totani (2005), taking into account the dispersion of the peak B band luminosity and the light-curve versus peak luminosity relation. We assume an extinction corresponding to the reddening $E(B-V) = 0.05$, which is reasonable for old galaxies and often used in rate studies of SNe Ia [see Oda et al. (2008) and references therein]. We assume the standard Milky-Way extinction curve. It should be noted

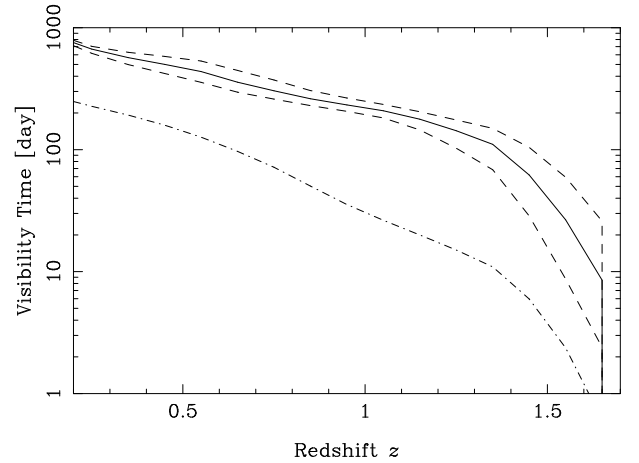


Fig. 6. The visibility time T_V (in observer's frame) of SNe in SXDS as a function of redshift. The solid curve is for the standard case of SNe Ia, while the dot-dashed curve is for CC SNe. The dashed curves are for SNe Ia, but the luminosity is shifted by ± 0.4 mag. The visibility time is slightly different in the different subfields of SXDS, and those in the SXDS-C field (Morokuma et al. 2008a) are shown here.

that the Calzetti *attenuation* law used in the photo- z calculations is for the synthesized flux from a galaxy, which is different from the *extinction* law for a single star in a galaxy. Therefore A_V of a galaxy estimated by photo- z calculation cannot be directly related to extinction of a SN in the galaxy. The effect of changing extinction of SN flux will be examined in section 4. The calculated visibility time is shown in Fig. 6.

The expected number of CC SNe, $N_{\text{CC,exp}}$, can be calculated as

$$N_{\text{CC,exp}} = \sum_i f_{\text{off},i} \psi_i f_{\text{CC}} \frac{T_{V,\text{CC}}(z_i)}{(1+z_i)} , \quad (4)$$

where ψ is SFR (mass per unit time) of a galaxy, and f_{CC} the production efficiency of CC SNe per unit mass of star formation. The SFR ψ is estimated by the ob-

served B band flux corresponding to the restframe UV luminosity, with the conversion factor calculated by the stellar population synthesis model used in this work. The factor f_{CC} is calculated by assuming that all stars heavier than $8 M_{\odot}$ produce CC SNe with the assumed IMF. The visibility time $T_{V,\text{CC}}$ is calculated with a standard mixture of light curves of various types of CC SNe, as in Oda & Totani (2005). We assume $E(B - V) = 0.15$ for CC SNe, which is a typical value for CC SNe found in nearby galaxies (Oda et al. 2008 and references therein). This value is larger than that assumed for SNe Ia, but it is reasonable since CC SNe are expected to occur in star forming regions where dust abundance is generally high. Since we selected old galaxies, we found $N_{\text{CC,exp}} = 11.4$ (in all the considered range of $t_{\text{Ia}} = 0.1\text{--}8$ Gyr) and this is small compared with $N_{\text{obs}} = 65$. (See also Table 2 for numbers in each t_{Ia} bin.)

The DTD estimated by this simple formulation is shown by open squares in Fig. 7, after converting the stellar mass of galaxies into the K -band luminosity $L_{K,0}$ that the galaxies would have at the age of 11 Gyr after passive evolution. The conversion is performed by calculating $M/L_{K,0}$ from the SED templates used in the photo- z calculations. We made this conversion because we can avoid some uncertainties in the stellar mass estimates, e.g., recycling or contribution from faint low-mass stars, by the normalization with K -band luminosity rather than stellar mass. A comparison with other observational DTD estimates also becomes easier. We assume that the stellar age of nearby elliptical galaxies is 11 Gyr as inferred from observations (e.g., Barber et al. 2007; Jimenez et al. 2007), and hence the observed SN Ia rate per unit K luminosity in nearby elliptical galaxies, $0.035^{+0.013}_{-0.011} (h/0.75)^2 \text{ century}^{-1} (10^{10} L_{K,\odot})^{-1}$ (Mannucci et al. 2005), gives an estimate of $f_D(11 \text{ Gyr})$, which can directly be compared with our estimates. This value is based on the rate measurement of Cappellaro et al. (1999) assuming $H_0 = 75 \text{ km/s/Mpc}$, and it is translated into a value for $h = 0.7$ used in this work.

Though these DTD results are derived by simply assuming $t_{\text{Ia}} = \langle t_* \rangle$, they are not significantly different from our final results shown by the filled squares (see below), and well described by a power-law, $f_D(t_{\text{Ia}}) \propto t_{\text{Ia}}^{\alpha}$ with $\alpha \sim -1$ in $0.1\text{--}11$ Gyr. However, to get a more accurate estimate, we make a correction as follows.

3.2. Correction for the Delay Time Estimates

In the above formulation, we simply estimated t_{Ia} of an observed SN Ia by $\langle t_* \rangle$ of its host galaxy. However, in reality, there is a probability distribution of t_{Ia} , which is determined by the DTD and star formation history $\psi(t)$, where $t = t_{\text{ga}} - t_{\text{Ia}}$ is the time elapsed from the beginning of the star formation in the host galaxy. The expectation value of the Ia delay time, $\langle t_{\text{Ia}} \rangle$, is exactly the same as $\langle t_* \rangle$ only when $f_D(t_{\text{Ia}})$ is constant against t_{Ia} . The expectation value is generally given by:

$$\langle t_{\text{Ia}} \rangle = \frac{\int_0^{t_{\text{ga}}} t_{\text{Ia}} \psi(t_{\text{ga}} - t_{\text{Ia}}) f_D(t_{\text{Ia}}) dt_{\text{Ia}}}{\int_0^{t_{\text{ga}}} \psi(t_{\text{ga}} - t_{\text{Ia}}) f_D(t_{\text{Ia}}) dt_{\text{Ia}}}. \quad (5)$$

Therefore, a more accurate estimate is obtained by the same formulation but with a summation over galaxies satisfying $t_l \leq \langle t_{\text{Ia}} \rangle < t_u$. However, this integration diverges when $t_{\text{Ia}} \rightarrow 0$ if $\alpha \leq -1$. The possibility of a significant population of the prompt SNe Ia with $t_{\text{Ia}} \lesssim 0.1$ Gyr has been discussed in recent years (Scannapieco & Bildsten 2005; Mannucci et al. 2006; Sullivan et al. 2006; Aubourg et al. 2007). Such a prompt population may also affect the estimate of the delay time. Therefore, we separate the prompt population (defined by $t_{\text{Ia}} < t_p = 0.1$ Gyr) from the tardy population ($t_{\text{Ia}} \geq t_p$). Then, the DTD of the tardy component can be estimated by a modified equation of eq. (1),

$$N_{\text{Ia,exp}} + N_{\text{pIa,exp}} + N_{\text{CC,exp}} = N_{\text{obs}}, \quad (6)$$

where $N_{\text{Ia,exp}}$ is now for the tardy population and the integration of eq. (5) is from $t_{\text{Ia}} = t_p$ to t_{ga} . The expected number of the prompt Ia, $N_{\text{pIa,exp}}$, can be calculated from SFR as for the case of $N_{\text{CC,exp}}$, if the integrated DTD at $0 \leq t_{\text{Ia}} \leq t_p$ is given.

A difficulty in this new formulation is that we need to know $f_D(t_{\text{Ia}})$ to calculate $\langle t_{\text{Ia}} \rangle$ and $N_{\text{pIa,exp}}$, before we make an estimate of $f_D(t_{\text{Ia}})$. In fact, this circularity problem can be solved easily; first we estimate f_D with an initial guess of $f_D(t_{\text{Ia}})$, and then we can iteratively repeat this process with the new estimate of $f_D(t_{\text{Ia}})$. The first DTD estimate with a constant f_D prior (open squares in Fig. 7) is well described by a power-law ($\propto t_{\text{Ia}}^{\alpha}$) at $t_{\text{Ia}} \geq t_p$, and hence we assume this form of f_D for the tardy population at the later iterations. For the prompt population, we make a reasonable assumption of a constant DTD at $t_{\text{Ia}} \leq t_p$ that is continuously connected to the tardy component, for every iteration. This is reasonable also from the DTD predictions by the stellar evolution theory (section 5).

We get sufficiently convergent results by just a few iterations of this procedure, and they are shown by filled squares in Fig. 7 as our final results. The error bars are statistical 1σ errors, which are calculated by the confidence limits of the small number Poisson statistics (Gehrels 1986). Since we selected old galaxies, $\langle t_* \rangle$ is already a good estimate of $\langle t_{\text{Ia}} \rangle$, and this is why the correction is not large. The expected number of the prompt population, $N_{\text{pIa,exp}}$, is 3.3 for the entire range of $t_{\text{Ia}} = 0.1\text{--}8$ Gyr, which is just 5.1% of the 65 SN candidates. The derived DTD, as well as important quantities such as $N_{\text{pIa,exp}}$, $N_{\text{CC,exp}}$, and N_{obs} , are summarized in Table 2 for the six time bins in $t_{\text{Ia}} = 0.1\text{--}8$ Gyr. The best fit power-law to the measured DTD is $f_D(1 \text{ Gyr}) = 0.53^{+0.12}_{-0.11} \text{ century}^{-1} (10^{10} L_{K,\odot,0})^{-1}$ and $\alpha = -1.06^{+0.15}_{-0.15}$. Here, we included the data point at $t_{\text{Ia}} = 11$ Gyr in the fit.

4. Examination of Systematic Uncertainties

4.1. Are the SN candidates really SNe Ia?

In our statistical estimation of DTD, it is not necessary to prove that all of the SN candidates are SNe Ia. Since we have already shown that the selected variable objects

Table 2. The DTD measurements by the baseline analysis. The DTD results are shown in $[\text{century}^{-1}]$ for a single starburst population whose total K band luminosity is $10^{10} L_{K,\odot}$ at an age of 11 Gyr. The errors are statistical 1σ . The number of old galaxies (N_{gal}), that of the detected SN candidates (N_{obs}), and the expected numbers of the prompt SNe Ia ($N_{\text{pIa,exp}}$) and CC SNe ($N_{\text{CC,exp}}$) are shown. The last column shows the mean of $\sigma_{t_{\text{Ia}}}$ of galaxies in a time bin, where $\sigma_{t_{\text{Ia}}}$ is the standard deviation of the probability distribution of t_{Ia} in a galaxy.

t_{Ia} bin [Gyr]	DTD $f_D(t_{\text{Ia}})$	N_{gal}	N_{obs}	$N_{\text{pIa,exp}}$	$N_{\text{CC,exp}}$	$\langle\sigma_{t_{\text{Ia}}}\rangle$ [Gyr]
0.1–0.25	$2.41^{+1.46}_{-1.08}$	3715	11	1.0	2.8	0.05
0.25–0.5	$2.07^{+0.92}_{-0.71}$	3073	15	0.85	3.0	0.14
0.5–1.0	$0.80^{+0.29}_{-0.23}$	4255	19	0.82	3.0	0.30
1.0–2.0	$0.45^{+0.15}_{-0.12}$	4781	19	0.61	2.3	0.50
2.0–4.0	$0.12^{+0.35}_{-0.12}$	565	1	0.046	0.20	1.2
4.0–8.0	$0.00^{+0.97}_{-0.00}$	103	0	0.008	0.038	2.1

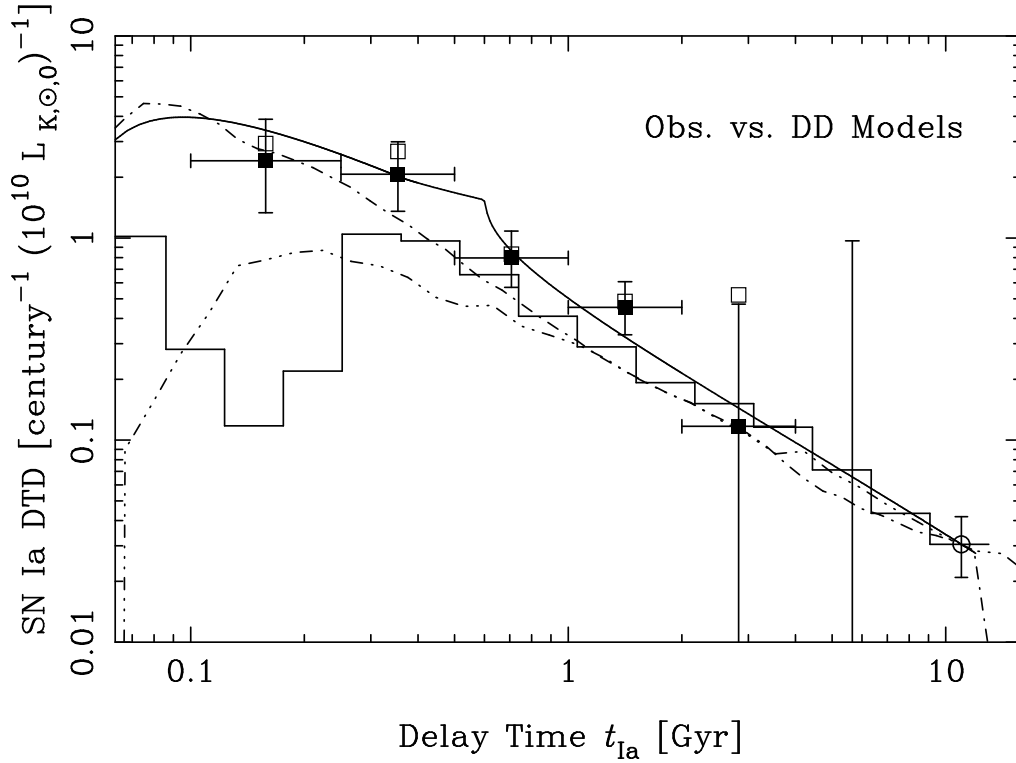


Fig. 7. The delay time distribution (DTD) of SNe Ia per unit delay time, t_{Ia} (century^{-1}), for a single starburst population whose total K -band luminosity is $10^{10} L_{K,\odot}$ at the age of 11 Gyr. The filled squares are the final observational estimates by this work, and the error bars are statistical 1σ errors. The open squares are the same but using a simpler method to estimate the delay time. (The error bars are not shown for these.) The open circle is DTD inferred from the SN Ia rate in elliptical galaxies in the local universe (Mannucci et al. 2005). The theoretical predictions based on the DD scenario by Ruiz-Lapuente & Canal (1998, three-dot-dashed), Yungelson & Livio (2000, dot-dashed), Greggio (2005, solid curve), and Belczynski et al. (2005, solid histogram) are also shown. The model curves are normalized by the DTD data at $t_{\text{Ia}} = 11$ Gyr.

are tracing the light profile of host galaxies, the majority of them must be SNe Ia or CC SNe. What we need to demonstrate is, then, that about 82% of the 65 candidates are actually SNe Ia, as inferred from the estimate of $N_{\text{CC,exp}} = 11.4$.

We first examine the i' band variability magnitude $m_{\text{var},i'}$ of the 65 SN candidates, and compare with the brightest magnitude $m_{\text{min},i'}$ that is possible for SNe Ia corresponding to the peak luminosity. We calculated this magnitude assuming the standard type Ia light curve with the mean peak B magnitude used in Oda & Totani (2005). We find that most (61/65) of the SN candidates have $m_{\text{var},i'} > m_{\text{min},i'}$ as expected, and all objects satisfy $m_{\text{var},i'} \geq m_{\text{min},i'} - 0.53$. The four objects with $m_{\text{var},i'} < m_{\text{min},i'}$ are reasonable considering the dispersion of the peak B magnitude of SNe Ia (~ 0.4 mag). On the other hand, about half of the SN candidates have the variability magnitudes brighter than $m_{\text{min},i'} + 1$, and such variability cannot be explained by CC SNe, because most of them are fainter than SNe Ia by 1–2 magnitudes (see e.g., Oda & Totani 2005).

We already made the DTD estimates, and we can predict the expected distribution of redshifts and stellar masses of host galaxies for the SN candidates, because we can calculate the expected number of SNe Ia in each galaxy. Comparison of these expected distributions with those observed provides us with an important consistency check of our DTD estimates. Figure 8 shows such comparisons, and the predictions based on our final DTD estimates are in nice agreement with the data. In the calculation of the expected redshift and stellar mass distributions, the light curve information of SNe is included through the visibility time. Therefore, we do not expect such an agreement, if our estimate of Ia/CC ratio is wrong or there is a significant contamination from any non-SN objects. In fact, the predicted distributions are in serious contradiction with the data if we assume that all the SN candidates are CC SNe. The agreement between the expected and observed distributions are quantitatively tested by the Kolmogorov-Smirnov test, and the results are given in Table 3. Acceptable fits are obtained both for the redshift and stellar mass distributions only when we make an appropriate mix of the tardy/prompt Ia and CC SNe with the relative proportions predicted by our DTD estimates, $N_{\text{exp}} = 45.4$, (tardy Ia) 3.3, (prompt Ia), and 11.4 (CC). These results then give a strong support to the reliability of our DTD estimates.

It should also be noted that we selected all variable objects associated with the old galaxies with a significant offset from the nuclei. Only 2 objects were removed by AGN-like variability, which is a negligible number compared with the final 65 candidates. Therefore, the true DTD cannot be larger than that derived by this work, and our DTD measurements would always be overestimates if there was any unknown contamination from non-SN objects.

Finally, we repeated our DTD estimates with a more stringent criteria for the old galaxies, $t_{\text{ga}}/\tau_{\text{SF}} \geq 3.0$, to select more efficiently SNe Ia rather than CC SNe. In

Table 3. The results of the Kolmogorov-Smirnov tests for the redshift and host galaxy stellar mass distributions of the SN candidates. The chance probabilities of getting the observed distributions are shown. (See Fig. 8 for the graphical presentations of these distributions.) The columns 2–4 show the results when all SNe are assumed to be tardy SNe Ia, prompt SNe Ia, and CC SNe, respectively. The last column shows the results when the three populations are mixed with the expected numbers (45.4, 3.3, and 11.4) in our baseline analysis.

	tardy Ia	prompt Ia	CC	mix
redshift	0.09	0.81	0.05	0.45
stellar mass	0.04	0.07	0.04	0.44

this case, the number of the SN candidates reduces to 44, but now $N_{\text{CC,exp}} = 5.4$ and $N_{\text{pIa,exp}} = 1.5$, and hence the expected Ia (tardy+prompt) fraction is increased to 88% from 82% in the baseline analysis. The DTD estimates and the power-law fit in this case are shown in Table 4, and there is no systematic trend from the baseline analysis.

4.2. Estimates of $\langle t_{\text{Ia}} \rangle$ and contribution from the prompt Ia population

In our analysis, the delay time t_{Ia} of each SN candidate has been estimated simply by the expectation value of $\langle t_{\text{Ia}} \rangle$ from the star formation history of the host galaxy. We have already shown that the difference between $\langle t_{\text{Ia}} \rangle$ and the mean stellar age $\langle t_* \rangle$ is small and does not seriously affect the final results. However, the probability distribution of t_{Ia} should have some dispersion around $\langle t_{\text{Ia}} \rangle$, and if this dispersion is larger than the bin width of the DTD estimate, it could affect the results. The dispersion around $\langle t_{\text{Ia}} \rangle$, $\sigma_{t_{\text{Ia}}} = (\langle t_{\text{Ia}}^2 \rangle - \langle t_{\text{Ia}} \rangle^2)^{1/2}$ is therefore calculated for each host galaxy in a similar way to eq. (5), and their average in a t_{Ia} bin is shown in Table 2. The dispersions are typically about half of the bin widths, and hence the binning size of our DTD estimates is appropriate.

In our baseline analysis, the amount of prompt SNe Ia is calculated by assuming a constant $f_D(t_{\text{Ia}})$ at $t_{\text{Ia}} \leq t_p$, and in this case the fraction of the prompt Ia is about 20% of all SNe Ia when the DTD is integrated over a range of $t_{\text{Ia}} = 0$ –11 Gyr. However, since we selected old galaxies, $N_{\text{pIa,exp}} = 3.1$ is just 5.1% of our 65 SN candidates. Therefore, our result will not be seriously affected by changing the prompt fraction, unless we assume an extremely higher prompt Ia rate (e.g., by a factor of about 10) than that assumed in the baseline analysis. We show the results of the DTD estimate when the prompt Ia population is enhanced by a factor of 2.5 from our baseline analysis in Table 4. In this case, the prompt fraction integrated over $t_{\text{Ia}} = 0$ –11 Gyr becomes $\sim 50\%$, which is a typical value discussed in recent papers about prompt SNe Ia (e.g., Mannucci et al. 2006; Sullivan et al. 2006). Our estimates of the tardy DTD is not seriously affected.

4.3. Systematic Uncertainties in Galaxy Ages

The age estimate of the host galaxies is crucial in our DTD estimates. Since we selected old or passively evol-

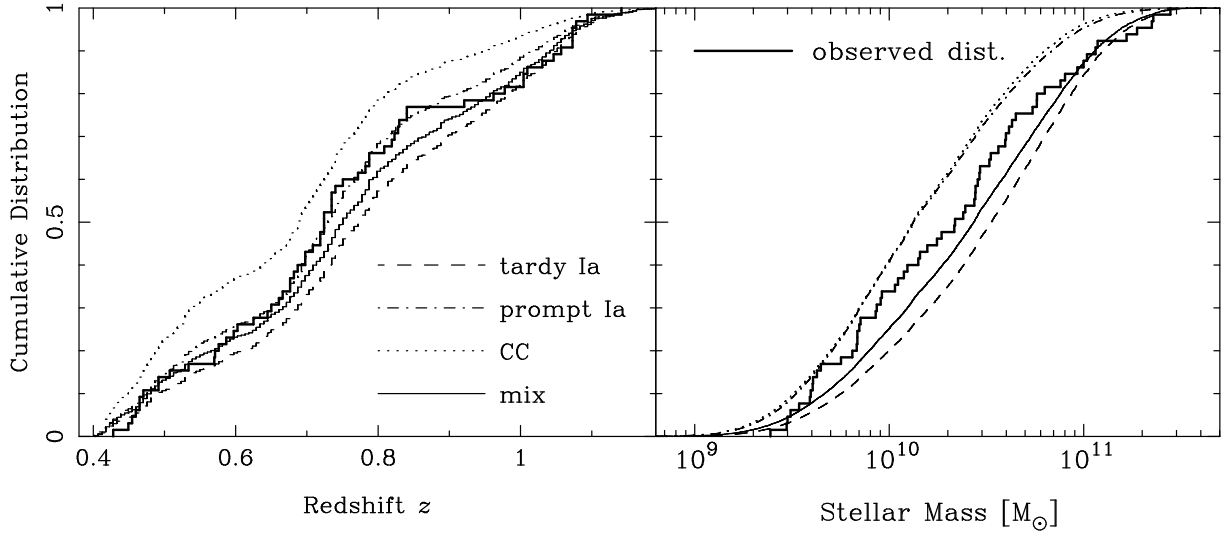


Fig. 8. The cumulative distributions of redshift and stellar mass of host galaxies for the SN candidates. The thick solid lines are the observed distributions of the 65 SN candidates. The dashed and dot-dashed curves are the expected distributions for the tardy ($t_{\text{Ia}} \geq 0.1$ Gyr) and prompt ($t_{\text{Ia}} < 0.1$ Gyr) components of SNe Ia, respectively, and the dotted curve is that for CC SNe. The thin solid curve is our best guess, which is the sum of the three components with the expected numbers in the baseline analysis: $N_{\text{exp}} = 45.4$ (tardy Ia), 3.3 (prompt Ia), and 11.4 (CC). The results of the Kolmogorov-Smirnov test for these distributions are given in Table 3.

Table 4. Examination of systematic errors in the DTD measurements. Various DTD results are shown when the analysis method is changed from the baseline analysis. The last two columns show the best-fit power-law DTD, $f_D(t_{\text{Ia}}) = f_{D, 1\text{Gyr}}(t_{\text{Ia}}/1 \text{ Gyr})^\alpha$. The “ $t_{\text{Ia}} = \langle t_* \rangle$ ” results are obtained by estimating t_{Ia} simply by mean stellar age $\langle t_* \rangle$ of the host galaxy (open squares in Figs. 7 and 10). The “ $t_{\text{ga}}/\tau_{\text{SF}} \geq 3.0$ ” results are obtained when a more strict criterion of the old galaxies is applied than the baseline analysis. The “prompt $\times 2.5$ ” results are obtained when the fraction of the prompt Ia population is increased by a factor of 2.5 from the baseline analysis. The “solar Z ”, “Chabrier IMF” and “KA97” results are obtained using the galaxy age estimates with a different metallicity, a different IMF, and a different stellar population synthesis model from the baseline analysis, respectively. The “SN ± 0.3 mag” results are obtained with the SN Ia light curve ± 0.3 mag fainter/brighter than in the baseline analysis. All errors are in statistical 1σ .

Analysis	$f_D(t_{\text{Ia}})$ [century $^{-1}(10^{10}L_{K,\odot,0})^{-1}$] in t_{Ia} bins [Gyr]						$f_{D, 1\text{Gyr}}$	α
	0.1–0.25	0.25–0.5	0.5–1.0	1.0–2.0	2.0–4.0	4.0–8.0		
baseline	2.41 $^{+1.46}_{-1.08}$	2.07 $^{+0.92}_{-0.71}$	0.80 $^{+0.29}_{-0.23}$	0.45 $^{+0.15}_{-0.12}$	0.12 $^{+0.35}_{-0.12}$	0.00 $^{+0.97}_{-0.00}$	0.53 $^{+0.12}_{-0.11}$	-1.06 $^{+0.15}_{-0.15}$
$t_{\text{Ia}} = \langle t_* \rangle$	2.93 $^{+1.54}_{-1.14}$	2.68 $^{+1.18}_{-0.89}$	0.83 $^{+0.34}_{-0.26}$	0.49 $^{+0.15}_{-0.12}$	0.52 $^{+0.39}_{-0.25}$	0.00 $^{+0.44}_{-0.00}$	0.60 $^{+0.13}_{-0.11}$	-1.07 $^{+0.15}_{-0.15}$
$t_{\text{ga}}/\tau_{\text{SF}} \geq 3.0$	5.22 $^{+4.97}_{-3.01}$	3.08 $^{+1.72}_{-1.24}$	0.79 $^{+0.31}_{-0.24}$	0.43 $^{+0.16}_{-0.12}$	0.16 $^{+0.43}_{-0.16}$	0.00 $^{+1.10}_{-0.00}$	0.61 $^{+0.16}_{-0.13}$	-1.21 $^{+0.18}_{-0.17}$
prompt $\times 2.5$	2.24 $^{+1.50}_{-1.12}$	1.63 $^{+0.89}_{-0.68}$	0.73 $^{+0.28}_{-0.23}$	0.43 $^{+0.16}_{-0.12}$	0.11 $^{+0.36}_{-0.11}$	0.00 $^{+0.95}_{-0.00}$	0.48 $^{+0.12}_{-0.10}$	-1.04 $^{+0.17}_{-0.15}$
solar Z	1.45 $^{+0.72}_{-0.55}$	1.58 $^{+0.80}_{-0.60}$	0.66 $^{+0.40}_{-0.29}$	0.58 $^{+0.18}_{-0.15}$	0.44 $^{+0.28}_{-0.19}$	0.25 $^{+0.68}_{-0.24}$	0.47 $^{+0.12}_{-0.10}$	-0.87 $^{+0.14}_{-0.14}$
Chabrier IMF	2.47 $^{+1.29}_{-0.97}$	2.13 $^{+0.93}_{-0.71}$	0.78 $^{+0.28}_{-0.22}$	0.35 $^{+0.14}_{-0.11}$	0.30 $^{+0.47}_{-0.23}$	0.00 $^{+0.89}_{-0.00}$	0.49 $^{+0.12}_{-0.10}$	-1.06 $^{+0.15}_{-0.14}$
KA97	1.10 $^{+0.51}_{-0.39}$	1.63 $^{+0.45}_{-0.38}$	0.42 $^{+0.27}_{-0.19}$	0.31 $^{+0.19}_{-0.13}$	0.28 $^{+0.31}_{-0.17}$	0.45 $^{+1.09}_{-0.39}$	0.36 $^{+0.09}_{-0.08}$	-0.87 $^{+0.14}_{-0.13}$
SN +0.3 mag	2.69 $^{+1.63}_{-1.20}$	2.34 $^{+1.05}_{-0.81}$	0.89 $^{+0.32}_{-0.25}$	0.51 $^{+0.17}_{-0.14}$	0.13 $^{+0.40}_{-0.13}$	0.00 $^{+1.06}_{-0.00}$	0.58 $^{+0.13}_{-0.12}$	-1.09 $^{+0.15}_{-0.15}$
SN -0.3 mag	2.16 $^{+1.31}_{-0.97}$	1.83 $^{+0.82}_{-0.63}$	0.71 $^{+0.25}_{-0.20}$	0.40 $^{+0.14}_{-0.11}$	0.10 $^{+0.31}_{-0.10}$	0.00 $^{+0.85}_{-0.00}$	0.48 $^{+0.11}_{-0.10}$	-1.03 $^{+0.15}_{-0.15}$

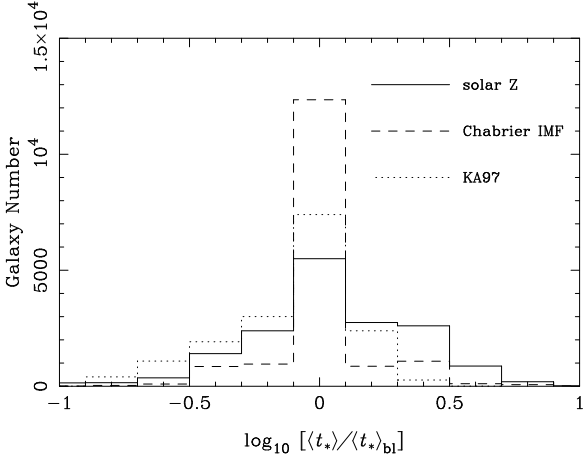


Fig. 9. The histogram of the mean stellar ages of the old galaxies estimated by alternative photometric redshift calculations to the baseline analysis. The stellar age is shown in the ratio to that in the baseline analysis. The solid and dashed lines are for the cases of changing to the solar metallicity ($Z = 0.02$) and to the Chabrier IMF, respectively. The dotted line is for the age estimate based on a completely different model (KA97) of stellar population synthesis.

ing galaxies in a relatively bright magnitude range of $m_i \leq 24$, the age estimate is expected to be easier than general studies of high- z galaxies. However, the age estimate may sensitively depend on the assumed star formation history, IMF, and metallicity in the photometric redshift calculation. Therefore the systematic uncertainties must be carefully examined.

In Fig. 9, we show the distribution of $\langle t_* \rangle / \langle t_* \rangle_{\text{bl}}$, i.e., the ratios of the mean stellar ages of the old galaxies with different prescriptions of photometric redshift calculations, to those in our baseline analysis. We tested the two cases of changing the metallicity into the solar abundance ($Z = 0.02$) and changing IMF into the Chabrier (2003) IMF, from the baseline analysis. Furthermore, we used a completely different population synthesis model by Kodama & Arimoto (1997, hereafter KA97), based on an independent stellar spectrum library. We used the $M_V = -21.98$ model of the metallicity-sequence KA97 models as a template. In this model, a gas infall and galactic wind are taken into account rather than a simple exponential SFR evolution, and the chemical evolution is solved in a self consistent manner. We have only one template for the star formation history, and hence the age estimate is not as accurate as the baseline analysis, but we can check the dependence on different stellar population synthesis models. It can be seen that the fractional change is within 10% for most galaxies, and the dispersion of $\log_{10}[\langle t_* \rangle / \langle t_* \rangle_{\text{bl}}]$ is 0.35, 0.23, and 0.27 for the cases of the solar abundance, the Chabrier IMF, and the KA97 model, respectively.

To examine the sensitivity of our DTD estimates to the age uncertainties, we repeated the DTD estimates but with $\langle t_{\text{Ia}} \rangle$ modified by the scaling of $\langle t_* \rangle / \langle t_* \rangle_{\text{bl}}$ for the three cases, and the results are shown in Table 4. The change in the DTD is within the statistical 1σ errors of

the baseline results for most of the data points.

We have removed the nuclear region of host galaxies within 1.9 pix radius in our SN candidate search, and it might induce some biases if the removed nuclear regions have considerably different stellar age from the outer regions. The mean fraction of i' flux in the nuclear region of the old galaxies is 0.35 in the total isophotal flux, and hence the outer regions are more dominant than the nuclear regions in the photometric redshift calculation. Figure 3 indicates that most of the old galaxies have elliptical morphologies, and they are likely to be the ancestors of the present-day elliptical galaxies (Yamada et al. 2005). It is known that the radial color gradient of local elliptical galaxies is explained by metallicity gradient rather than age gradient (Tamura et al. 2000). The typical metallicity gradient is $d \log Z / d \log r \sim 0.3$ (Kobayashi & Arimoto 1999), and hence the effect of metallicity gradient has already been tested, at least partially, by the above examination of the age dependence on metallicity.

4.4. Systematic Uncertainties in Supernova Luminosity

The light curves of SNe are essential for calculations of the visibility time and hence for a rate study. We used the standard light curves of various supernova types as in Oda & Totani (2005). However, we selected SNe Ia in galaxies with old stellar population, and a systematic trend that SNe Ia in old stellar population is fainter than those in star forming galaxies by a peak magnitude difference of $\Delta M_B \sim 0.3$ has been known (Gallagher et al. 2005; Sullivan et al. 2006).

The effect of extinction may also change the apparent luminosity of SNe. We assumed a low extinction of $E(B - V) = 0.05$ (or $A_V = 0.155$ for the standard Milky Way extinction curve), which is reasonable for old galaxies. However, this value is smaller than $\langle A_V \rangle = 0.31$ of the old galaxies estimated by the photo- z code, though this value should not directly be compared with the extinction of SN flux, as mentioned in section 3.1. It should also be noted that the distribution of old galaxy A_V is strongly peaked at $A_V = 0$ (Fig. 1), and the uncertainty in A_V estimate may have resulted in a larger $\langle A_V \rangle$ than the real value.

To examine the sensitivity of the DTD estimates to the change of SN luminosity by these effects, we repeated the DTD estimates with the SN Ia light curve shifted by ± 0.3 mag, and the results are shown in Table 4. The results are not much different from the baseline analysis, and the uncertainty about the SN luminosity is unlikely to change our main conclusions significantly.

5. Implications for the SN Ia Progenitor

5.1. the Double-Degenerate Scenario

The DTDs predicted by the four different theoretical models (Ruiz-Lapuente & Canal 1998; Yungelson & Livio 2000; Greggio 2005; Belczynski et al. 2005) based on the DD scenario are also shown in Fig. 7. The model curves are normalized at the data point of $t_{\text{Ia}} = 11$ Gyr for presentation, but the normalization should be regarded as a

free parameter and we should compare the DTD shape between the observations and the models. It is impressive that the predictions by different authors are very close, and in excellent agreement with the observed DTD at $t_{\text{Ia}} \gtrsim 0.2$ Gyr. It is not surprising that different authors made similar predictions, because it is a robust and generic prediction of the DD scenario as argued below.

A common feature for DTD models based on this scenario is that the delay time is mainly determined by the time t_{GW} from the formation of a DD binary (i.e., a binary of two white dwarfs) to a merger after the angular momentum loss by gravitational wave radiation, especially in the long delay time range of $t_{\text{Ia}} \gtrsim 1$ Gyr. The general relativity tells us $t_{\text{Ia}} \sim t_{\text{GW}} \propto a^4$, where a is the initial separation of the DD binary. If the separation distribution is given by $f_{\text{sep}}(a) \propto a^\beta$, the DTD should be

$$f_D(t_{\text{Ia}}) \propto f_{\text{sep}}(a) \frac{da}{dt_{\text{Ia}}} \propto t_{\text{Ia}}^{-(3-\beta)/4}, \quad (7)$$

and hence $\alpha = -(3 - \beta)/4$. It is known that the distribution of initial binary separation a_0 at the time of binary star formation is approximately flat in $\log a_0$, i.e., $f_{\text{sep},0}(a_0) \propto a_0^{-1}$ (Abt 1983). Although there is a significant change and contraction of binary separations during the evolution from a binary star formation to a DD binary (e.g., Greggio 2005), it would be reasonable to assume $\beta \sim -1$ also for the initial separation of DD binaries. Then we expect $\alpha \sim -1$, as found in the DTD models based on the DD scenario. Though β for DD binaries is rather uncertain and model-dependent, the dependence of α on β is small. Furthermore, the range of the delay time from 0.1 to 10 Gyr corresponds to a range of a only by a factor of 3.2. Therefore, if a is smoothly distributed in this narrow range, we expect a power-law DTD with $\alpha \sim -1$ in wide and general conditions. This is a general result applicable to all merging phenomena triggered by gravitational wave radiation, such as binary neutron star mergers (Totani 1997), and this is why the DTD models by different authors are quite similar to each other, especially at large delay times. The agreement of the measured DTD with this generic prediction gives a strong support for the DD scenario.

In Fig. 7, we selected the standard DTD model when a few models based on the DD scenario are presented by a single author group [the standard DDS model of Belczynski et al. (2005) and the close-DD model of Greggio (2005)]. The variation models predict slightly different value of α , but smooth power-law like DTDs are always common predictions, as expected from the above consideration.

On the other hand, the difference between the DTD predictions by different authors becomes bigger at short delay time ($t_{\text{Ia}} \lesssim 0.1$ Gyr), where the delay time is dominated by stellar evolution time scale rather than t_{GW} . There are large uncertainties in the treatments of stellar evolution in binary population synthesis, and the discrepancy between some of the DTD models and the observed data at this short t_{Ia} range is not serious for the DD scenario.

5.2. the Single-Degenerate Scenario

The measured DTD is compared with the theoretical models based on the SD scenario in Fig. 10. Again, the normalization of the models is arbitrary, and we should compare only the shape of the DTD function. In contrast to the DD scenario, the predictions by this scenario are quite different depending on different authors. It is common to this scenario that the delay time is essentially determined by the main-sequence life time of the secondary star in a binary, because other time scales (e.g., accretion phase onto the white dwarf) are much shorter. However, the DTD models shown in this figure are calculated by considerably different methods with a wide range of complexity.

The predictions by Matteucci et al. (2006) and the $Z = 0.05$ model of Kobayashi & Nomoto (2008, hereafter KN08) are close to a simple power-law, and they are relatively in good agreement with the observed DTD, compared with other models. However, it should be noted that the two models are based on the simplest calculations among the models shown here, though such a simple analytical approach is useful in applications for e.g. studies of chemical evolution in galaxies (Kobayashi et al. 1998; Matteucci & Recchi 2001; Matteucci et al. 2006; KN08). In these calculations, the condition for a binary system to evolve to a SN Ia event (i.e., stable accretion up to the Chandrasekhar mass) is determined by the initial masses of the primary and secondary stars, regardless of the binary separation. If the masses are in acceptable ranges, a binary evolves into a SN Ia with a constant efficiency, and no SN Ia is produced in other mass ranges. In such a calculation, the DTD shape is determined by IMF and the distribution of the primary/secondary mass ratio. If smooth functions are assumed for these, a smooth DTD without a characteristic scale of t_{Ia} is obtained. However, a constant SN Ia efficiency within an extended mass range is likely to be an oversimplification. The SN Ia condition should be determined by the combination of the stellar masses and binary separation, and it is natural to expect that there are some characteristic secondary mass scales preferred for successful SN Ia events, which should appear as particular time scales in DTD, rather than a power-law like DTD.

There are two distinct populations of the main-sequence donor channel (WD+MS) and the red-giant donor channel (WD+RG) for short and long delay times, respectively, in the KN08 model based on the progenitor model of Hachisu et al. (1996, 2008). The relative abundances of the two are determined empirically by fitting to the chemical evolution data, rather than by theoretical modeling. Therefore, the good agreement of the KN08 model with our DTD estimate may partially be a result of this feedback from other observations, indicating that our DTD estimate is also consistent with the chemical evolution data. It would be rather surprising if distinct two populations contribute at similar levels and form a featureless DTD. Though the WD+MS channel is widely considered as the promising SD progenitor of SNe Ia, the SN Ia rate theoretically ex-

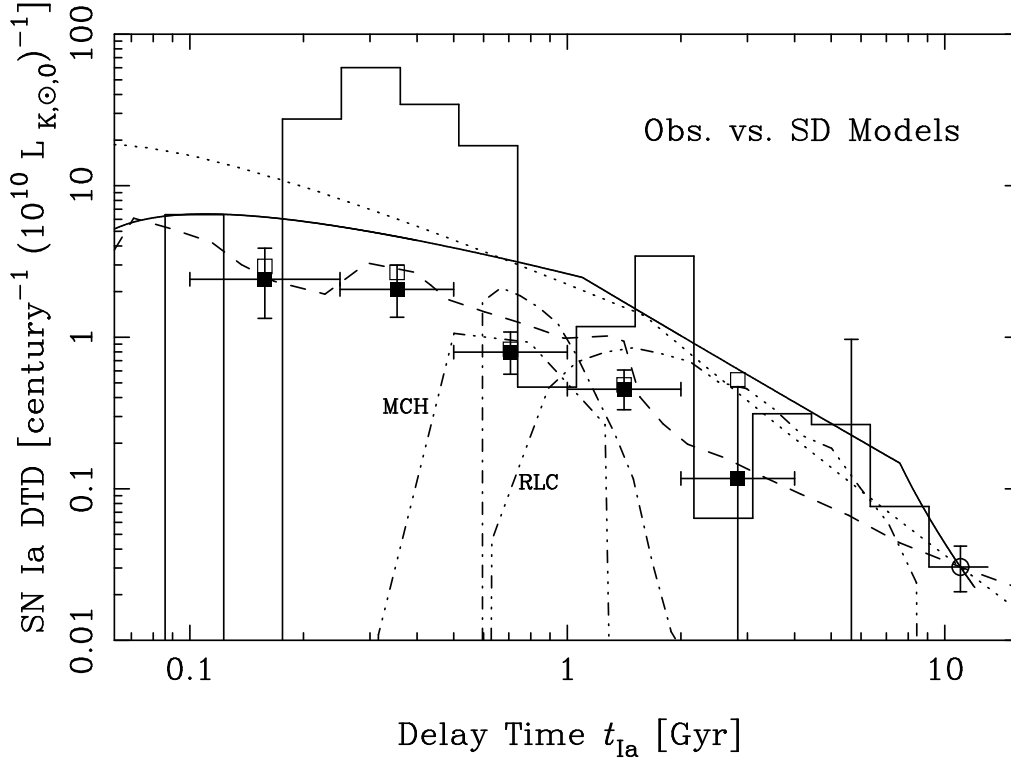


Fig. 10. The same as Fig. 7, but for a comparison with the DTD predictions based on the SD scenario. The predictions of Greggio (2005, solid curve), Matteucci et al. (2006, dotted), and Kobayashi & Nomoto (2008, dashed) are based on analytic models. The predictions of Ruiz-Lapuente & Canal (1998, three-dot-dashed with the label “RLC”), Yungelson & Livio (2000, dot-dashed), Belczynski et al. (2005, solid histogram), and Meng et al. (2008, three-dot-dashed with the label “MCH”) are based on binary stellar population synthesis calculations. The model curves are normalized by the DTD data at $t_{\text{Ia}} = 11$ Gyr when they are non-zero, otherwise the normalization is arbitrary.

pected from the WD+RG channel is much lower than that of the WD+MS channel (Yungelson & Livio 1998; Han & Podsiadlowski 2004; Meng et al. 2008).

The SN Ia condition is determined only by stellar masses also in the standard SD-Chandra model of Greggio (2005), but the mass budget of the accretion from the donor to the white dwarf up to the Chandrasekhar mass is treated in more detail. An interesting feature is the sharp drop of DTD at a large delay time of $\gtrsim 8$ Gyr. SNe Ia with such a large delay time are produced from binary systems with a small secondary mass. Since such a low mass star has a small mass of the envelope that can be used for the accretion onto the companion white dwarf, the mass of the primary star must be large enough to ensure that the initial white dwarf mass is sufficiently massive and the white dwarf successfully grows to the Chandrasekhar mass. Therefore the number of binaries that can evolve to SNe Ia rapidly decreases with decreasing secondary mass. It seems difficult to reproduce a single power-law like DTD up to ~ 10 Gyrs if this effect is incorporated.

Finally, predictions of the SG-Ch model of Yungelson & Livio (2000), the standard SDS model of Belczynski et al. (2005), the CLS model of Ruiz-Lapuente & Canal (1998), and the model of Meng et al. (2008) ($\alpha_{\text{CE}} = 3$ and $Z = 0.03$) are shown, which are based on detailed calculations of the binary population synthesis, where the calculations start from the initial conditions including the

primary and secondary stellar masses and the binary separation. There are a number of parameters and uncertain physical processes in such calculations, and different conditions for SNe Ia are assumed by different authors, leading to very different DTD predictions. However, a clear trend is that some characteristic scales of the delay time appear in the DTD, making the DTD shape more complex than the simple analytic models. This is reasonable in realistic conditions, as argued above, and it is theoretically unlikely that a simple power-law like DTD is obtained in the framework of the SD scenario.

6. Summary and Conclusions

We directly measured the delay time distribution (DTD) of type Ia supernovae in the delay time range of $t_{\text{Ia}} = 0.1\text{--}8$ Gyr by using the statistics of the faint variable objects detected in the systematic variable object survey performed as a part of the Subaru/XMM-Newton Deep Survey project.

We selected 16,492 old galaxies having low SFR compared with their stellar mass (i.e., low specific SFR), in the redshift range of $0.4 \leq z_{\text{ph}} \leq 1.2$. We then selected variable objects associated with these galaxies but having significant offsets from the nuclei of galaxies, to remove the contamination of AGNs. We found 65 variable objects, whose locations with respect to their host galaxies

closely trace the profiles of galactic light, and hence the majority of them must be supernovae. Though we do not have spectroscopic confirmation of the SN types, we quantitatively demonstrated that the majority ($\gtrsim 80\%$) of the SN candidates should be SNe Ia, based on the variability luminosity, redshift distribution, and properties of the host galaxies.

Combined with the observed SN Ia rate in elliptical galaxies in the local universe, we derive the SN Ia DTD in a range of $t_{\text{Ia}} = 1\text{--}11$ Gyr, and found that it can well be described by a simple power-law, $f_D(t_{\text{Ia}}) \propto t_{\text{Ia}}^\alpha$ with $\alpha \sim -1$. We performed various tests about the systematic uncertainties in this DTD measurement, but the changes of DTD estimates are not large enough to change our main conclusions significantly.

The derived DTD at $t_{\text{Ia}} \gtrsim 0.2$ Gyr is in excellent agreement with the theoretical predictions based on the DD scenario. The theoretical predictions by different authors are very similar to each other, and a featureless power-law shape is inevitable consequence of the general relativity in this scenario. Therefore we consider that the agreement between the observed and predicted DTDs gives a strong support to this scenario. It indicates that the major contributor to SNe Ia is the DD channel for delay times larger than $t_{\text{Ia}} \gtrsim 0.1$ Gyr, although some contribution from other channels cannot be excluded.

On the other hand, the predictions by the competing SD scenario are vastly different for different authors. Although the predicted DTDs based on simple analytical approaches have smooth shapes which are broadly consistent with our measurement, predictions based on more detailed binary population synthesis calculations show strong peaks in the DTD shape, which do not fit the observed DTD. This trend can naturally be understood; if there is any preferred scale of the secondary stellar mass in a binary for successful evolution to a SN Ia, it should be reflected as a characteristic delay time scale in this scenario. Therefore we consider that our result does not favor the SD scenario in general as the major channel to the tardy SN Ia population ($t_{\text{Ia}} \gtrsim 0.1$ Gyr). There are many degrees of freedom and uncertainties in the theoretical modeling based on the SD scenario, and it would be premature to reject the SD scenario simply from our result. However, our result should set a stringent constraint on the model parameter space, if the SD channel is responsible for the majority of the tardy SNe Ia. It is highly desirable to examine physical effects and evolutionary paths that are not taken into account in existing models of binary population synthesis.

In the literature, it has occasionally been argued that the SD scenario is more favored than the DD scenario, but arguments against the DD scenario are not particularly strong. A merger of two white dwarfs may result in an accretion induced collapse rather than a SN Ia (Saio & Nomoto 1985), but theoretical uncertainties are still quite large (Piersanti et al. 2003; Yoon et al. 2007). Many binary systems are proposed as candidates of the SN Ia progenitor in the SD framework, compared with the observed number of DD binaries that can evolve

to SNe Ia (Parthasarathy et al. 2007). However, DD binaries are difficult to detect and the statistics of the DD binary search is not sufficient yet to confirm or reject the DD scenario (Tovmassian et al. 2004; Geier et al. 2007; Napiwotzki 2007). There are some implications for the progenitor from studies of SN Ia remnants (Ruiz-Lapuente et al. 2004; Badenes et al. 2007; Ihara et al. 2007), or from spectroscopic studies (Leonard 2007; Patat et al. 2007a, b; Simon et al. 2007) and archival progenitor searches (Voss & Nelemans 2008; Nelemans et al. 2008; Roelofs et al. 2008) of nearby SNe Ia. However, conclusive results from these studies have not yet been obtained, mainly because of the limited statistics and theoretical uncertainties.

Recent studies (Scannapieco & Bildsten 2005; Sullivan et al. 2006; Aubourg et al. 2007) have tried to model the DTD by two components: the prompt component and the constant f_D component against t_{Ia} . Although our result does not put a strong constraint on the amount of the prompt component, a constant f_D seems to be an oversimplification for the tardy component, since $f_D(t_{\text{Ia}})$ at an intermediate delay time of $t_{\text{Ia}} \sim 1$ Gyr is about 10 times larger than $f_D(11 \text{ Gyr})$. It should be noted that the prompt Ia population is a considerable fraction ($\sim 20\%$) when the DTD inferred from our observation is integrated over $t_{\text{Ia}} = 0\text{--}11$ Gyr, if we make a modest assumption that $f_D(t_{\text{Ia}})$ at $t_{\text{Ia}} < 0.1$ Gyr is constant at the value of $f_D(0.1 \text{ Gyr})$. Most of the observed data of SN Ia rate dependence on galaxy properties can be reproduced by DTD models based on the DD scenario (Greggio 2005; Mannucci et al. 2006). The possible enhancement of SN Ia rate in radio galaxies may require an even higher prompt Ia fraction than that expected from our data or the DD scenario (Della Valle et al. 2005; Mannucci et al. 2006), but the statistics of this enhancement is still small and must be confirmed by future observations.

We would like to thank K. Belczynski, R. Canal, L. Greggio, F. Matteucci, X. Meng, P. Ruiz-Lapuente, and L. R. Yungelson for providing numerical data of their DTD models. This work is based in part on the observations made with the Subaru Telescope operated by the National Astronomical Observatory of Japan, the Spitzer Space Telescope operated by the Jet Propulsion Laboratory, California Institute of Technology under a contract with NASA of the U.S.A., and the United Kingdom Infrared Telescope operated by the Joint Astronomy Centre on behalf of the Science and Technology Facilities Council of the U.K. A part of the optical imaging and spectroscopic data were obtained as a part of the Supernova Cosmology Project. This work was supported in part by the Grant-in-Aid for Scientific Research (19740099, 19035005) and for the 21st Century COE ‘‘Center for Diversity and Universality in Physics’’ from the Ministry of Education, Culture, Sports, Science and Technology (MEXT) of Japan. This work was also supported in part by the Core-to-Core Program ‘‘International Research Network for Dark Energy’’ and the Japan-USA Bilateral Program of the Japan Society for Promotion of Science

(JSPS).

References

- Abt, H.A. 1983, *ARA&A*, 21, 343
- Aubourg, E., Tojeiro, R., Jimenez, R., Heavens, A.F., Strauss, M. A., Spergel, D. N. 2007, submitted to *ApJL*, arXiv:0707.1328
- Badenes, C., Hughes, J. P., Bravo, E., & Langer, N. 2007, *ApJ*, 662, 472
- Barber, T., Meiksin, A., & Murphy, T. 2007, *MNRAS*, 377, 787
- Barris, B. J., & Tonry, J. L. 2006, *ApJ*, 637, 427
- Belczynski, K., Bulik, T., & Ruiter, A. J. 2005, *ApJ*, 629, 915
- Blanc, G. & Greggio, L. 2008, to appear in *New Astron.* (arXiv:0803.3793)
- Bolzoni, M., Miralles, J.-M., & Pell, R. 2000, *A&A*, 363, 476
- Bruzual, G., & Charlot, S. 2003, *MNRAS*, 344, 1000
- Calzetti, D., Armus, L., Bohlin, R. C., Kinney, A. L., Koornneef, J., & Storchi-Bergmann, T. 2000, *ApJ*, 533, 682
- Cappellaro, E., Evans, R., & Turatto, M. 1999, *A&A*, 351, 459
- Chabrier, G. 2003, *PASP*, 115, 763
- Dahlen, T. et al. 2004, *ApJ*, 613, 189
- Della Valle M., Panagia N., Padovani P., Cappellaro E., Mannucci F., Turatto M., 2005, *ApJ*, 629, 750
- Förster, F., Wolf, C., Podsiadlowski, Ph., & Han, Z. 2006, *MNRAS*, 368, 1893
- Furusawa, H. et al. 2008, *ApJS* in press (arXiv:0801.4017)
- Gallagher, J. S., Garnavich, P. M., Berlind, P., Challis, P., Jha, S., & Kirshner, R. P. 2005, *ApJ*, 634, 210
- Gal-Yam, A. & Maoz, D. 2004, *MNRAS*, 347, 942
- Gehrels, N. 1986, *ApJ*, 303, 336
- Geier, S., Nesslinger, S., Heber, U., Przybilla, N., Napiwotzki, R., & Kudritzki, R.-P. 2007, *A&A*, 464, 299
- Greggio, L. 2005, *A&A*, 441, 1055
- Hachisu, I., Kato, M., & Nomoto, K. 1996, *ApJ*, 470, L97
- Hachisu, I., Kato, M., & Nomoto, K. 2008, *ApJ* in press (arXiv:0710.0319)
- Han, Z., & Podsiadlowski, Ph. 2004, *MNRAS*, 350, 1301
- Hillebrandt, W., & Niemeyer, J. C. 2000, *ARA&A*, 38, 191
- Iben, I. Jr. & Tutukov, A. V. 1984, *ApJS*, 84, 335
- Ihara, Y., Ozaki, J., Doi, M., Shigeyama, T., Kashikawa, N., Komiyama, K., & Hattori, T. 2007, *PASJ*, 59, 811
- Jimenez, R., Bernardi, M., Haiman, Z., Panter, B., & Heavens, A. F. 2007, *ApJ*, 669, 947
- Kobayashi, C., Tsujimoto, T., Nomoto, K., Hachisu, I., & Kato, M. 1998, *ApJ*, 503, L155
- Kobayashi, C., & Arimoto, N. 1999, *ApJ*, 527, 573
- Kobayashi, C., & Nomoto, K. 2008, submitted to *ApJ* (arXiv:0801.0215) (KN08)
- Kodama, T., & Arimoto, N., 1997, *A&A*, 320, 41 (KA97)
- Leonard, D. C. 2007, *ApJ*, 670, 1275
- Livio, M. 2001, in “Supernovae and gamma-ray bursts: the greatest explosions since the Big Bang” (eds M. Livio, N. Panagia, K. Sahu), 334 (Cambridge Univ. Press, Cambridge) (arXiv:astro-ph/0005344)
- Lonsdale, C. et al. 2004, *ApJS*, 154, 54
- Mannucci, F., Della Valle, M., Panagia, N., Cappellaro, E., Cresci, G., Maiolino, R., Petrosian, A., Turatto, M. 2005, *A&A*, 433, 807
- Mannucci, F., Della Valle, M., & Panagia, N. 2006, *MNRAS*, 370, 773
- Maoz, D. & Gal-Yam, A. 2004, *MNRAS*, 347, 951
- Matteucci, F., & Recchi, S. 2001, *ApJ*, 558, 351
- Matteucci, F., Panagia, N., Pipino, A., Mannucci, F., Recchi, S., & Della Valle, M. 2006, *MNRAS*, 372, 265
- Meng, X., Chen, X., & Han, Z. 2008, submitted to *MNRAS* (arXiv:0802.2471)
- Morokuma, T. et al. 2008a, *ApJ*, 676, 167
- Morokuma, T. et al. 2008b, *ApJ*, 676, 121
- Napiwotzki, R. 2007, in “15th European Workshop on White Dwarfs” (eds R. Napiwotzki and M.R. Burleigh), 387 (ASP Conference Series Vol. 372, Astronomical Society of the Pacific, San Francisco, 2007)
- Nelemans, G., Voss, R., Roelofs, G., & Bassa, C. 2008, submitted to *MNRAS* (arXiv:0802.2239)
- Nomoto, K. 1982, *ApJ*, 253, 798
- Nomoto, K., Iwamoto, K., & Kishimoto, N. 1997, *Sci*, 276, 1378
- Oda, T., & Totani, T. 2005, *ApJ*, 630, 59
- Oda, T., Totani, T., Yasuda, N., Sumi, T., Morokuma, T., Doi, M., & Kosugi, G. 2008, *PASJ* in press (arXiv:0801.2194)
- Parthasarathy, M., Branch, D. Jeffery, D. J., & Baron, E. 2007, *New Astron. Rev.* 51, 524
- Patat, F. 2007a, *Science*, 317, 924
- Patat, F. 2007b, *A&A*, 474, 931
- Perlmutter, S. et al. 1999, *ApJ*, 517, 565
- Piersanti, L., Gagliardi, S. Iben, I. Jr., & Tornamb, A. 2003, *ApJ*, 598, 1229
- Poznanski, D. et al. 2007, *MNRAS*, 382, 1169
- Riess, A. G. et al. 1998, *AJ*, 116, 1009
- Roelofs, G., Bassa, C., Voss, R., & Nelemans, G. 2008, submitted to *MNRAS* (arXiv:0802.2097)
- Ruiz-Lapuente, P., & Canal, R. 1998, *ApJ*, 497, L57
- Ruiz-Lapuente, P., et al. 2004, *Nature*, 431, 1069
- Saio, H. & Nomoto, K. 1985, *A&A*, 150, L21
- Scannapieco, E., & Bildsten, L. 2005, *ApJ*, 629, L85
- Sérsic, J. L. 1968, *Atlas de galaxies australes* (Cordoba, Argentina: Observatorio Astronomico)
- Simon, J. D. et al., 2007, *ApJ*, 671, L25
- Strolger, L.-G. et al. 2004, *ApJ*, 613, 200; 635, 1370 (E)
- Sullivan, M., et al. 2006, *ApJ*, 648, 868
- Tamura, N., Kobayashi, C., Arimoto, N., Kodama, T., & Ohta, K. 2000, *AJ*, 119, 2134
- Totani, T. 1997, *ApJ*, 486, L71
- Tovmassian, G. H., Napiwotzki, R., Richer, M. G., Stasiska, G., Fullerton, A. W., & Rauch, T. 2004, *ApJ*, 616, 485
- Voss, R., & Nelemans, G. 2008, *Nature*, 451, 802
- Warren, S. et al. 2007, *MNRAS*, 375, 213
- Webbink, R. 1984, *ApJ*, 277, 355
- Whelan, J., & Iben, I. Jr. 1973, *ApJ*, 186, 1007
- Yamada, T. et al. 2005, *ApJ*, 634, 861; 659, 862 (E)
- Yoon, S.-C., Podsiadlowski, Ph., & Rosswog, S. 2007, *MNRAS*, 380, 933
- Yungelson, L., & Livio, M. 1998, *ApJ*, 497, 168
- Yungelson, L.R., & Livio, M. 2000, *ApJ*, 528, 108